Modelling of Cut-off Frequency of Armchair Graphene Nanoribbon Tunnel Field Effect Transistor Using Transfer Matrix Method

Endi Suhendi[1*], Jaka Brajadenta[1], Ahmad Aminudin[1], Dadi Rusdiana[1]

[1]Program Studi Fisika, Universitas Pendidikan Indonesia, 40154, Bandung, Indonesia.

ABSTRACT

Graphene is considered as a promising two-dimensional material for electronic device applications due to its high charge carrier mobility and it is extremely thin in size. As a material, graphene has great potential for the development of high-speed nano electric devices. Graphene can be used as a channel material in Tunnel Field Effect Transistor (TFET). In this study, the cut-off frequency of the armchair graphene nanoribbon tunnel field effect transistor (AGNR-TFET) device was modelled quantum mechanically. The solution of the Dirac-like Hamiltonian and Poisson equations self-consistently is used to determine the potential profile of device and the transmittance is calculated using the transfer matrix method (TMM). The Landauer formulation with the help of Gauss Legendre Quadrature Method (GLQM) is used to calculate the tunnelling current and the cut-off frequency of AGNR-TFET. The calculation results showed that the cut-off frequency increased as the drain voltage increased, while the increase in channel length and the N-index graphene made the cut-off frequency decreased. Moreover, the thicker the oxide layer could increase the cut-off frequency and the higher the temperature on the device would reduce the cut-off frequency.

1. INTRODUCTION

Graphene is a material consisting of a single layer of carbon atoms with a hexagonal lattice that was first created in 2004 by Konstantin Novoselov and Andre Geim from graphite using the Scotch-tape method [1]. This material has become prominent due to its unique physical properties. Graphene has an electron mobility of up to 200,000 cm^2/(V·s) [2], the energy band gap can be varied between 0 – 0.8 eV [3] and its size is relatively very thin when compared to silicon semiconductors with electron mobility of 1,400 cm^2/(V·s) [4] and energy band gap 1.1 eV [5]. Based on this, graphene has advantages as a new material for making electronic components, one of which is transistors. Graphene with a certain width (w) and length (L) so that it is shaped like a ribbon is often referred to as graphene nanoribbon (GNR). Based on the cut edge, GNR is divided into two types, namely armchair (AGNR) and zigzag (ZGNR). The two types will show different characteristics of graphene, ZGNR will show conductor properties and AGNR can show semiconductor properties depending on the width value [6]. AGNR can be developed and used in various electronic devices [7].

Some researchers have reported that monolayer graphene can be applied to tunnel field-effect transistors (TFET) for high-speed devices and radio frequency applications. They reported that TFET showed better performance with increasing cut-off frequency up to Gigahertz. However, there are some obstacles to be faced such as the rise of capacitance effect, the effect of size at the nanoscale, and the effect of self-heating on the device [8, 9, 10, 11, 12]. This paper reports the use

---

* Corresponding author: endis@upi.edu

of AGNR material in TFET and analyses the characteristics of its cut-off frequency value. The n-type AGNR-TFET is formed by three main channels, namely the source that is connected to a p⁺-type semiconductor, the gate that is connected to a n-type semiconductor and it is limited by the oxide material, and the drain is connected to a n⁺-type semiconductor. AGNR can become a p-type semiconductor when it is doped by boron or aluminium and can become an n-type semiconductor when it is doped by nitrogen or phosphorus [13, 14]. The synthesis of AGNR by given some doping was carried out using the modern chemical vapor deposition (CVD) method to make it more efficient [15].

In this paper, the calculations are carried out using the transfer matrix method (TMM). TMM is used because it can eliminate numerical deficiencies in other methods such as the Wentzel Kramers-Brillouin (WKB) approach and the Airy function approach [16, 17, 18, 19] and it is simpler than the use of the Non-Equilibrium Green's function (NEGF) method [9]. The Cut-off frequency (f_T) will be calculated and analysed based on the influencing parameters such as drain voltage (V_d), channel length (L_{ch}), N-index of AGNR, oxide layer thickness (t_{ox}), and device temperature (T).

2. THEORETICAL METHODS

The structure of the AGNR-TFET device tunneling current is shown in Figure 1 refers to [20]. The determination of the potential profile of AGNR-TFET is done by solving the Dirac-like Hamiltonian and Poisson equations self-consistently. The transmittance is calculated using TMM. The TMM is a numerical method that divides the potential profile of the AGNR-TFET into several segments to calculate the value of transmittance. The Landauer formulation with the help of Gauss Legendre Quadrature Method (GLQM) is used to calculate the tunneling current.
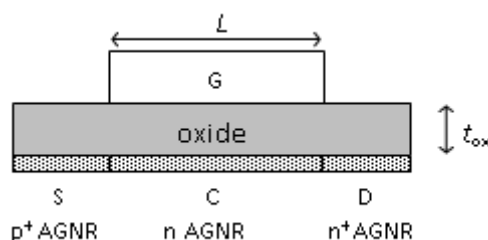
Figure 1. The device structure of the n-channel AGNR-TFET [20]

The cut-off frequency can be formulated in Equation (1) where g_m and C_g are the total transconductance and capacitance of the line, respectively.

$$f_T = \frac{g_m}{2\pi C_g} \tag{1}$$

A transconductance is defined by Equation (2) as the first derivative of the tunneling current function towards the gate voltage or the difference in tunneling current for each gate voltage change [7].

$$g_m = \partial I_d / \partial V_g \tag{2}$$

The total capacitance in the channel is formulated in Equation (3) which states the effect that arises due to the insulator layer so that polarization occurs at the gate assuming that the polarized charge is constant [10, 21, 22, 23].

$$C_g = C_{ox}WL \tag{3}$$

L is the length of the AGNR at the gate and C_{ox} is the capacitance in the oxide area or is formulated in Equation (4).

$$C_{ox} = \varepsilon_{ox}/t_{ox} \tag{4}$$

## 3. RESULTS AND DISCUSSION

The modelling results regarding the effect of changes in drain voltage towards the cut-off frequency are shown in Figure 2. The parameters used are as follows; the channel length in 20 nm, the width of N-index AGNR of 42, 1 nm of the oxide layer thickness at a temperature of 300 K.
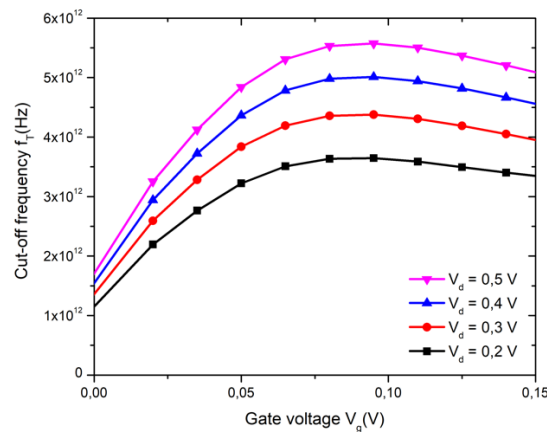
Figure 2. Cut-off frequency AGNR-TFET Vs. gate voltage with drain voltage variation

The relationship between the drain voltage and the resulting cut-off frequency is proportional to the higher drain voltage value that will result in a higher cut-off frequency peak. This could happen due to an increase in transconductance as a result of the wider energy band gap between the source valence band and drain conduction band which is in line with the findings of the study [24]. The highest cut-off frequency peak is 5.58 THz which occurs when a 0.5 V drain voltage is applied.

Figures 3 and 4 show the effect of the AGNR dimension on the cut-off frequency. Figure 3 shows the effect of channel length on the cut-off frequency. The width of N-index AGNR used is 42. The cut-off frequency decreases as the line length of the device increases. By the increase of the channel length, it can reduce transconductance due to slower electron travel time and increase in channel capacitance based on material geometry which results in more electrons being blocked and polarized in the channel as previously done in previous research [9].
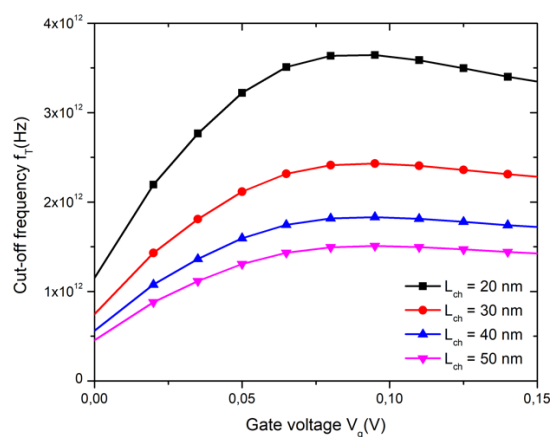
Figure 3. Cut-off frequency AGNR-TFET Vs. gate voltage with channel length variation

In addition, an exponential decrease occurs because the cut-off frequency is proportional to $1/\tau$ and it can be formulated by Equation (5).

$$f_T \propto 1/\tau = v_d/L_{ch} \tag{5}$$

where v_d is the electron drift velocity and it defined in Equation (6).

$$v_d = \mu_{eff}E_d \tag{6}$$

and E_d is the electric field generated by the drain electric potential, thus the cut-off frequency is expressed by the Equation (7) [25].

$$f_T \sim \left(\mu_{eff}V_D/L_{ch}\right)/L_{ch} \tag{7}$$

Figure 4 demonstrates the effect of the AGNR width expressed by the N-index indicator on the cut-off frequency. The channel length used is 20 nm. Figure 4 shows a decrease in the cut-off frequency as the N-index AGNR increases. This can happen because the effect of capacitance that occurs is greater than the increase in transconductance from the wider AGNR causing a decrease in the energy band gap. However, the change in the energy band gap is relatively small due to the difference in the N-index compared to the increase in capacitance that occurs. The increase in total capacitance results in more electrons in the channel because more charge is accumulated according to the cross-sectional area on the surface of the AGNR. Since the increase in the number of electrons that accumulate in the channel is much greater than the increase in the number of electrons in the drain, the ratio between drain and channel will decrease thereby reducing the cut-off frequency as the AGNR width increases [26].
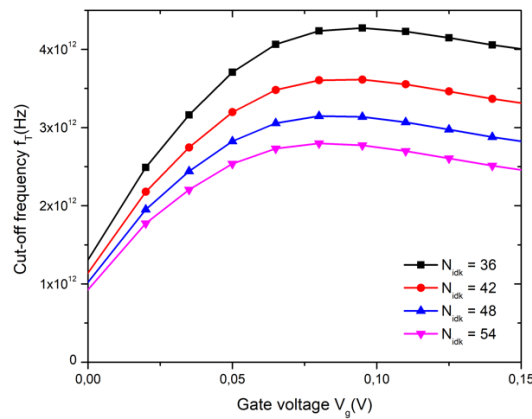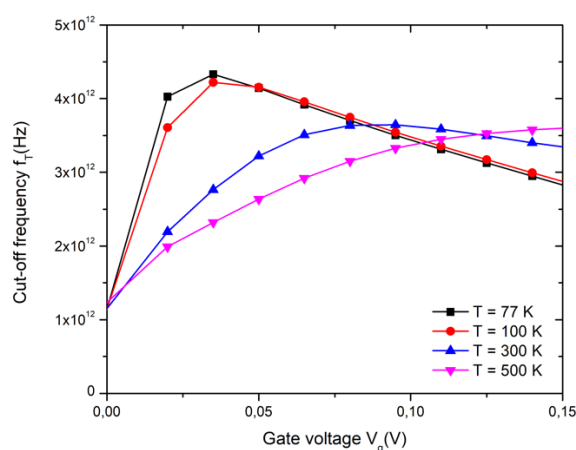
Figure 4. Cut-off frequency AGNR-TFET Vs. gate voltage with variation of N-index (width) AGNR

The increase in the peak cut-off frequency due to the increase in the thickness of the oxide layer is shown in Figure 5. The difference in the increase in the cut-off frequency with the increase in the thickness of the oxide layer in the figure appears to decrease since the total capacitance value decreases as the distance between the channel and the gate electric field source increases. On the other hand, the value of transconductance will decrease because the electric field of the gate voltage is less efficient in adjusting the energy band gap, therefore the potential barrier will be greater. This is in line with previous studies suggesting that there was an optimum value limit for the thickness of the oxide layer based on the entire device dimension structure [9].
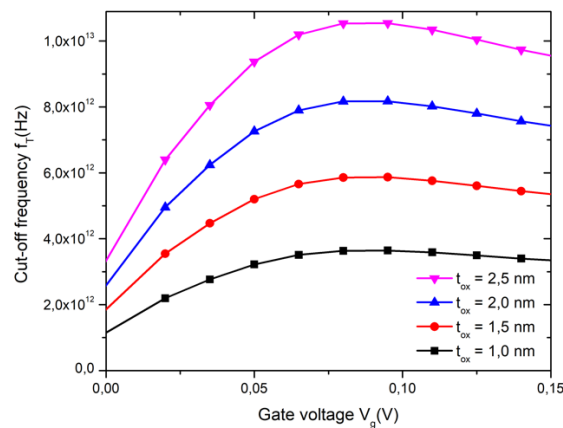
Figure 5. Cut-off frequency AGNR-TFET Vs. gate voltage with variation of oxide layer thickness.

Figure 6 shows the effect of variations in temperature conditions on the device with the same fixed parameters as before. It demonstrates the high cut-off frequency at low temperatures since the AGNR-TFET has a higher transconductance and charge carrier mobility [27]. At high temperatures, electrons will have greater kinetic energy and move randomly, so the possibility of collision is bigger. This collision can cause phonon scattering effects that have an impact on the stability of the charge carrier mobility, as in previous studies the electron mobility increases with increasing temperature at low temperature conditions. After that, the mobility of the charge carriers decreases with increasing temperature [28].

Figure 6. Cut-off frequency AGNR-TFET Vs. gate voltage with temperature variation.

4. CONCLUSION

The cut-off frequency on the AGNR-TFET continues to increase as the gate voltage increases until the saturation condition has a peak and finally decreases due to the effect of the resulting total capacitance. The effect of drain voltage on cut-off frequency is proportional because drain voltage can increase charge carrier mobility and transconductance. The length of the channel affects the travel time of electrons to the drain and the total capacitance value of the device increases. Thus, the cut-off frequency decreases as the channel length increases. This also happens when the width of the AGNR increases. The charge that reaches the drain increases; however, the charge that accumulates in the drain increases more. Hence, increasing the width of the AGNR will reduce the value of the cut-off frequency. Meanwhile, the thicker the oxide layer, the greater the total capacitance effect, although the resulting transconductance is also reduced. The cut-off frequency increases as the thickness of the oxide layer increases to a certain extent. At low temperatures the resistance in the device is smaller than at high temperatures and the electrons are easier to avoid collisions with other electrons or atomic nuclei. Therefore, the cut-off frequency produced at low temperatures is higher than at high temperatures.

REFERENCES

[1]   Geim, A., Novoselov, K., Nature Mater. vol **6**, (2007) pp. 183–191.

[2]   Bolotin, K. I., et al., Solid State Commun., vol. **146**, no. 9–10 (2008) pp. 351–355.

[3]   I. M. Marks and M. G. Gelder, Graphene Nanoelectronics, vol. 111, no. 479. Berlin, Heidelberg: Springer Berlin Heidelberg, 2012.

[4]   Jacoboni, C., Canali, C., Ottaviani, G., and Alberigi Quaranta, A., Solid. State. Electron., vol. **20**, no. 2, (1977) pp. 77–89.

[5]   Collings, P.J., Am. J. Phys., vol. **48**, no. 3, (1980) pp. 197–199.

[6]   Rozhkov, A. V., Savel'ev, S., and Nori, F., Phys. Rev. B, vol. **79**, no. 12, (2009) p. 125420.

[7]   Schwierz, F., Nat. Nanotechnol., vol. **5**, no. 7, (2010) pp. 487–496.

[8]   S. Dash, G. S. Sahoo, and G. P. Mishra, "Improved Cut-off Frequency for Cylindrical Gate TFET Using Source Delta Doping," Procedia Technol., vol. 25, no. December, (2016) pp. 450–455.

[9]   Chauhan, J., and Guo, J., Nano Res., vol. **4**, no. 6, (2011) pp. 571–579.

[10]   Pradhan, K. P., Mohapatra, S. K., Sahu, P. K., and Behera, D. K., Microelectronics J., vol. **45**, no. 2, (2014) pp. 144–151.

[11]   Sarvari, H., Ghayour, A. H., Chen, Z., and Ghayour, R., J. Mater., vol. **2016**, (2016) pp. 1–8.

[12]   Bonmann, M., et al., IEEE Trans. Electron Devices, (2020) pp. 1–8.

[13]   Nemnes, G. A., Mitran, T. L., Manolescu, A., and Dragoman, D., Phys. B Condens. Matter, vol. **561**, (2019) pp. 9–15.

[14]   Nemnes, G. A., Mitran, T. L., Manolescu, A., and Dragoman, D., Comput. Mater. Sci., vol. **155**, no. August, (2018) pp. 175–179.

[15]   Fujimoto, Y., and Saito, S., Surf. Sci., vol. **634**, (2015) pp. 57–61.

[16]   Li, W., IEEE J. Quantum Electron., vol. **46**, no. 6, (2010) pp. 970–975.

[17]   Jirauschek, C., IEEE J. Quantum Electron., vol. **45**, no. 9, (2009) pp. 1059–1067.

[18]   Bimo, C. S. P., Noor, F. A., Abdullah, M., and Khairurrijal, Adv. Mater. Res., vol. **896**, (2014) pp. 371–374.

[19]   Zhang, Q., Fang, T., Xing, H., Seabaugh, A., and Jena, D., IEEE Electron Device Lett, vol. **29**, no. 12, (2008) pp. 1344–1346.

[20]   Suhendi, E., Hasanah, L., Rusdiana, D., Noor, F.A., Kurniasih, N., and Khairurrijal, J. Semicond., vol. **40**, no. 6, (2019) p. 062002.

[21]   Wu, Y., et al., Nature, vol. **472**, no. 7341, (2011) pp. 74–78.

[22]   Lin, Y.-M., et al., vol. **327**, no. 5966, (2010) pp. 662–662.

[23]   Wu, Y., et al., Nano Lett., vol. **12**, no. 6, (2012) pp. 3062–3067.

[24]   Hwang, B.-W., Yeom, H.-I., Kim, D., Kim, C.-K., Lee, D., and Choi, Y.-K., Solid. State. Electron., vol. **141**, no. August 2017, (2018) pp. 65–68.

[25]   Lin, Y., Jenkins, K. A., Valdes-Garcia, A., Small, J. P., Farmer, D. B., and Avouris, P., Nano Lett., vol. **9**, no. 1, (2009) pp. 422–426.

[26]   Rawat B., and Paily, R., IEEE Trans. Nanotechnol., vol. **16**, no. 3, (2017) pp. 411–416.

[27]   Akbari Eshkalak, M., Iran. J. Electr. Electron. Eng., vol. **12**, no. 2, (2016) pp. 147–153.

[28]   Liu, Y., Li, W., Qi, M., Li, X., Zhou, Y., and Ren, Z., Phys. E Low-dimensional Syst. Nanostructures, vol. **69**, (2015) pp. 115–120.